PHYSICAL REVIEW LETTERS

Carrier Lifetime in Exfoliated Few-Layer Graphene Determined from Intersubband Optical Transitions

Thomas Limmer,[1] Jochen Feldmann,[1] and Enrico Da Como[2,*]

[1]*Photonics and Optoelectronics Group, Physics Department and CeNS, Ludwig-Maximilians-Universität München, Amalienstrasse 54, 80799 München, Germany*
[2]*Department of Physics, University of Bath, Claverton Down, BA2 7AY Bath, United Kingdom*
(Received 6 August 2012; published 23 May 2013)

We report a femtosecond transient spectroscopy study in the near to middle infrared range, 0.8–0.35 eV photon energy, on graphene and few layer graphene single flakes. The spectra show an evolving structure of photoinduced absorption bands superimposed on the bleaching caused by Pauli blocking of the interband optically coupled states. Supported by tight-binding model calculations, we assign the photo-induced absorption features to intersubband transitions as the number of layers is increased. Interestingly, the intersubband photoinduced resonances show a longer dynamics than the interband bleaching, because of their independence from the absolute energy of the carriers with respect to the Dirac point. The dynamic of these intersubband transitions reflects the lifetime of the hot carriers and provides an elegant method to access it in this important class of semimetals.

The recombination lifetime of charge carriers is the outmost important process when using semiconductors in optoelectronics [1]. Recombination controls light emission, lasing, and photocurrent generation in many different devices. For most semiconductors the recombination of charge carriers can be measured by monitoring their population at the band gap. Information about recombination can be achieved indirectly from the photoluminescence lifetime, provided the semiconductor exhibits radiative recombination, or the recovery of the ground-state absorption in photoinduced transient experiments (pump-probe), when the probe light is in resonance with the band gap. In recent years semimetals, or zero gap semiconductors, such as HgTe, graphene, and few-layer graphene have attracted a considerable interest both from a fundamental and applied viewpoint [2,3]. Few-layer graphene has been successfully implemented in fast photodiodes, satureable absorbers, and light modulators, promising to become a platform material for high speed optoelectronics [4–6]. While in all these applications the material carrier lifetime determines the ultimate performance, the gapless nature of these systems poses serious limits in assessing it using the conventional optical contactless techniques described above.

In this Letter, we show how it is possible to determine the hot carrier lifetime in few-layer graphene flakes by monitoring the dynamics of photoinduced intersubband transitions. The experiments are performed by means of femtosecond pump-probe spectroscopy with an octave spanning photon-energy range, 0.35 to 0.8 eV. At these photon energies we expect to be sensitive to the intersubband structure of few-layer graphene, which is known to become more complex as different layers are stacked one on top of the other [3,7,8]. The differential absorption

spectra are dominated by the bleaching (decreased absorption) of optically coupled interband transitions due to phase-space filling of states. However, 2-, 3-, 4-, and 5-layer graphene show photoinduced absorption features superimposed on the bleaching. In agreement with simulated spectra based on tight-binding model calculations, we assign the absorption features to intersubband optical transitions. As we demonstrate, their lifetime is linked to the presence of hot carrier distributions and provides an elegant method to access the hot carrier lifetime in few-layer graphene flakes.

Single and few-layer graphene flakes, with the typical *A-B* stacking sequence, were prepared by mechanical exfoliation of natural graphite and deposited on SiO_2 substrates. The homogeneity of the layers was checked by micro-Raman [9]. Single and few-layer homogeneous graphene flakes were then transferred to quartz to perform optical experiments on a transparent substrate with a low tendency of doping the flakes [10]. Even after this transfer the graphene layers did not show evidence of a *D* band in the Raman spectrum, testifying to the high quality of the flakes [11]. In addition, the position of the *G* band in the Raman spectra was recorded to assure the absence of heavily doped flakes (Fermi energy < 0.1 eV) [9,12,13]. Carriers were photoexcited with 100 fs pulses at 1.55 eV from an amplified Ti:sapphire laser. Probe pulses with similar time durations were obtained from an optical parametric amplifier (OPA). The signal and idler from the OPA were used as probe beams [14]. Experiments were performed by focusing the pump and probe beams on a single flake in ambient conditions and detecting the differential probe-beam absorption $\Delta a(t, \hbar\omega)$ at different time delays between the pump and the probe t, and different probe photon energies $\hbar\omega$. Experiments were conducted in a

linear regime between pump fluence and Δa signal ampli-tudes with photoinduced carrier densities of $\sim 10^{10}$ cm^{-2}.

Figures 1(a)–1(e) show the Δa spectra at different pump-probe time delays for each sample: 1-, 2-, 3-, 4-, and 5-layer graphene, respectively. Whereas the 1-layer graphene exhibits a featureless photoinduced bleaching $\Delta a < 0$ over the whole probe photon energy range due to Pauli blocking of interband transitions between optically coupled states, the few-layer graphene samples show photoinduced absorption bands with $\Delta a > 0$. In 3-, 4-, and 5-layer flakes, together with the absorption band above 0.6 eV, absorption features below 0.5 eV can be discerned superimposed to the bleaching. Two-layer graphene shows only a prominent resonance centered at 0.44 eV, whereas 4-layer two bands at 0.7 and 0.43 eV. In general, we observe a spectrum richer in absorption features which appear broader as the number of layers increases. Another important characteristic of these data lies in the *time domain*. By taking a closer look at the time evolution it is possible to recognize a longer lifetime of the absorp-tion features with respect to the bleaching signals. Spectra at 0.5 ps time delay between the pump and probe pulses

show the absorption bands with almost the same intensity of those at 0 ps, while the bleaching signal intensity is appreciably decreased.

We have first attempted to describe the nature of the absorption features appearing in the few-layer graphene spectra. We have used a tight-binding model to describe the electronic structure of graphene and few-layer graphene [7]. This allowed us to have an accurate estimation of how the band structure evolves as the number of graphene layers changes (Fig. 2(f)). Using the tight-binding wave functions we have then calculated the matrix elements for all possible transitions, first between the subband levels within the conduction and the valence band (intersubband transitions) and then for those occurring across the conduction and valence band (interband transitions) [9].

The simulated Δa spectra in Figs. 2(a)–2(e) are obtained by calculating the absorption spectra of graphene flakes at elevated carrier temperatures $a_{\mathrm{Exc}}(\hbar\omega)$ and subtracting the absorption at room temperature, $a_{\mathrm{RT}}(\hbar\omega)$. In doing this we have assumed an ultrafast (<100 fs) intersubband scatter-ing to the bottom (top) subband for electrons (holes).

FIG. 1 (color online). Transient absorption spectra recorded at different time delays between pump and probe for (a) 1-layer, (b) 2-layer, (c) 3-layer, (d) 4-layer, and (e) 5-layer graphene. Pump pulse centered at 1.55 eV. Spectra are recorded collecting transient signal decays at specific probe wavelengths indicated as data points and shown for three pump-probe delays: 0, 0.5, and 4 ps.
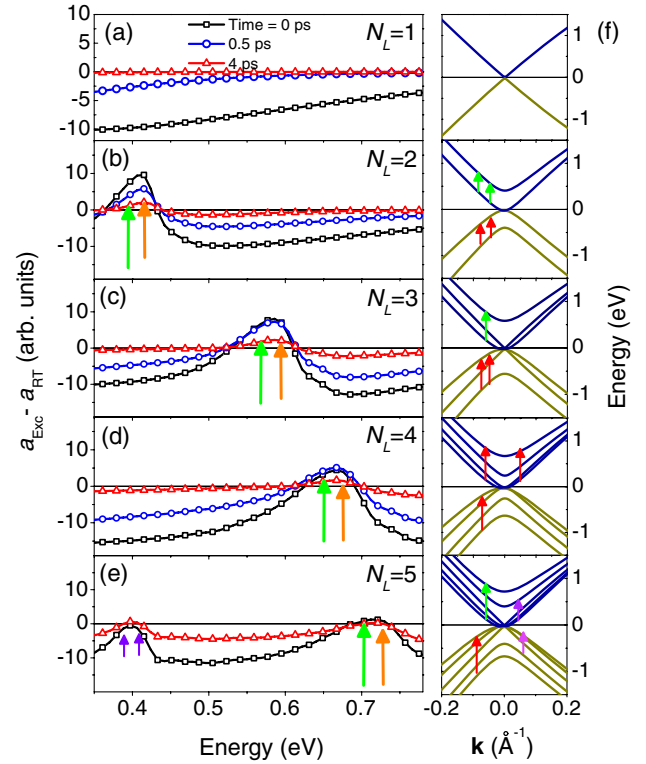
FIG. 2 (color online). Calculated transient absorption spectra for (a) 1-layer, (b) 2-layer, (c) 3-layer, (d) 4-layer, and (e) 5-layer graphene. The spectra are shown for three different times cor-responding to three different values of T_c for each sample. The specific T_c where obtained from the best fits of the experimental curves of Fig. 1 according to the procedure in Ref. [16]. The spectrum of each sample was obtained considering the respective band structure calculated with the tight-binding model and shown on the right column (f). The arrows indicate the respec-tive intersubband transitions at arbitrarily chosen **k** values.

In general $a(\hbar\omega)$ can be expressed as

$$a(\hbar\omega) \propto \sum_{j,f} \int \frac{d\mathbf{k}}{2\pi} \cdot |\langle \Psi^f(\mathbf{k})|\hat{F} \cdot \vec{P}|\Psi^j(\mathbf{k})\rangle|^2$$

$$\cdot \, \text{Im}\left[\frac{f(E^f(\mathbf{k}), T_c, \mu) - f(E^j(\mathbf{k}), T_c, \mu)}{E^f(\mathbf{k}) - E^j(\mathbf{k}) - \omega - i\Gamma}\right],$$

where the sum runs on all possible initial (j) and final (f) states, the first term under the integral, wave vector ($\mathbf{k}$) integration limits in the first Brillouin zone, is the matrix element for a dipole transition between the final $\Psi^f(\mathbf{k})$ and initial states, $\Psi^j(\mathbf{k})$ with $\hat{F}$ representing the electric field of radiation and $\vec{P}$ the electron momentum operator [9]. The second term under the integral expresses the resonance condition considering the Fermi functions $f(E^{f,j}(\mathbf{k}), T_c, \mu)$ for a specific energy E, carrier temperature T_c, and chemical potential μ. Γ is a broadening parameter [9,15]. To obtain the calculated spectra shown in Fig. 2 at the corresponding delay times of the experimental spectra, we used the cooling curves (T_c as a function of time) for 1- and 2-layer or estimated T_c at specific time delays [9]. T_c values and cooling curves have been extracted following a procedure published in one of our previous works [16]. From the cooling curves it is possible to estimate T_c at a specific time delay and use that value for calculating spectra with the equation above. The calculated spectra exhibit a good agreement with the measured Δa and, most important, they capture the structure of absorption resonances. We note small deviations on the low-energy side, below 0.4 eV, which might be due to intraband Drude-like absorption [16–18] and a down shift of 0.1 eV for the absorption transition of the 3-layer sample.

A first clear indication suggesting that photoinduced absorption resonances originate from intersubband transitions comes from their absence in single-layer graphene, where a subband structure is not present. The assignment of the intersubband absorption transitions is indicated by the corresponding vertical arrows in the respective energy dispersion diagrams. The 2-layer sample can undergo absorption transitions from the bottom subband to the top one, both in the conduction and valence band. The small but appreciable energy difference in the separation of subband levels of the conduction and valence band at the same $\mathbf{k}$ value is responsible for the asymmetry in the resonance peak, noticeable both in the experimental and modeled spectra. As the number is increased by one, a new couple of subbands are added and additional transitions contribute to the absorption resonances. A consequence is that absorption features are broadened and shifted at higher energy, the latter effect because of the increasing energy separation between the outermost subbands.

It is also important to notice how our simulated spectra reproduce the bleaching intervals in which hot carriers occupying the bottom-conduction and top-valence subbands induce Pauli blocking of optically coupled interband

transitions. This gives us confidence that our initial assumption of a fast intersubband scattering to the bottom (top) subband for electrons (holes) used in the model is valid and reflects the real experimental dynamics. In agreement with the experimental curves, the modeled absorption features appear to have a longer lifetime than the bleaching.

We now turn to the dynamics of the photoinduced absorption caused by intersubband transitions and the bleaching caused by Pauli blocking. Δa appears positive for intersubband and negative for bleaching, since the blocking of interband transitions corresponds to less absorption with respect to the system in the ground state (no pump). Figure 3(a) compares the Δa transients for the 2-layer sample at a probe energy of 0.42 eV, corresponding to the photoinduced absorption resonance, and at 0.66 eV which instead tracks the bleaching at this specific energy. While the bleaching has a bi-exponential decay with a first ultrafast almost resolution-limited decay of 0.2 ps and a second component of 2.8 ps, the intersubband absorption shows a monoexponential decay of 5 ps. In general, all the absorption features for all samples of Fig. 1 exhibit a monoexponential decay, which is often a factor of 2 longer than the second component of the bleaching at any of the
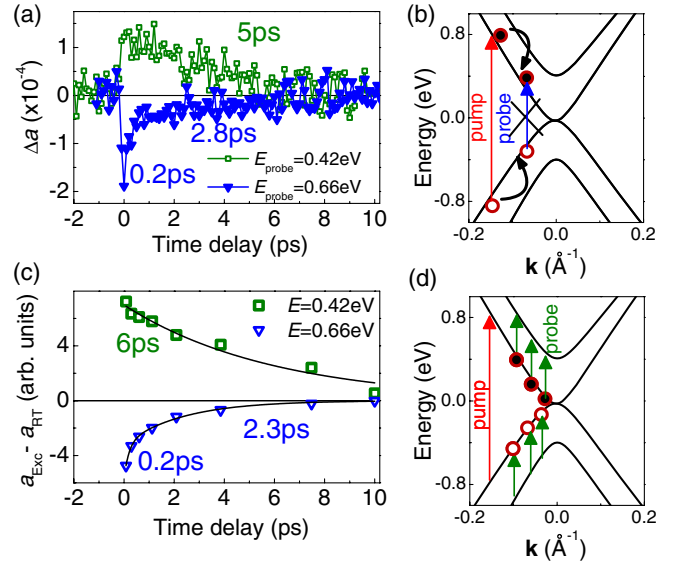
FIG. 3 (color online).   (a) Photoinduced transient decay of the intersubband absorption, 0.42 eV (green squares), and the photobleaching, 0.66 eV (blue triangles), in 2-layer graphene. (b) Illustration of the Pauli blocked interband transitions and carrier relaxation (curved arrows) superimposed on the calculated energy dispersion diagram for 2-layer graphene. (c) Transients obtained from the simulated differential absorption spectra of Fig. 2(b) at photon energies of 0.42 (green squares) and 0.66 eV (blue triangles). Solid lines are mono- and biexponential fits for the points. (d) Illustration of the intersubband absorption transitions superimposed on the calculated energy dispersion diagram for 2-layer graphene.

probe energies with $\Delta a < 0$. We can interpret this behavior according to the schemes in Figs. 3(b) and 3(d).

Figure 3(b) shows the band structure of 2-layer graphene with hot electrons (filled dots) and holes (empty dots) at different energies and **k** values. Such hot carriers relax in the respective bands by emission of optical and acoustic phonons until they reach a thermal equilibrium with the lattice [16,19,20]. Therefore, the lifetime probed by Pauli-blocked interband transitions corresponds to the rate at which the two Fermi-Dirac distributions describing hot carriers, one for electrons and one for holes, are depopulating those optically selected states and equilibrate close to the Dirac point. This means that bleaching signals monitor carrier distributions at a specific **k** far from the charge neutrality point which in our flakes is **k** ~ 0. The depopulation of states at a specific **k** is determined by several physical processes such as intraband relaxation by optical and acoustic phonons, Coulomb scattering, and eventually interband recombination [21,22]. Thus, it is difficult to extract reliable information on the carrier lifetime from the bleaching, since a number of processes are contributing to the recorded decay which has a signal vanishing without necessarily having the graphene carrier distribution equilibrated at room temperature. Often a typical biexponential curve is observed, which is ascribed to optical and acoustic phonon scattering [19].

In Fig. 3(d) we present a scheme of the intersubband transitions for electrons and holes in 2-layer graphene. Here, in contrast to bleaching signals, it is interesting to note how the presence of intersubband absorption transitions is *independent* from the energy of the carriers or their **k** with respect to the Dirac point. In other words, the decay of the intersubband photoinduced absorptions is only sensitive to the presence of a hot carrier distribution which differs from the one at room temperature. We assign the decay of the intersubband transitions to the hot carrier lifetime and propose this as a method to investigate the different recombination processes, which have been thus far proposed on the basis of theoretical models and investigated experimentally for epitaxial layers [20,22–24]. Within the range of carrier energies or temperatures explored in our study, the monoexponential nature of this decay points to one dominant recombination process.

In Fig. 3(c) we report the evolution of the calculated transient absorption signals as a function of time. Those were extracted from the spectra of Fig. 2(b) at the same photon energies of the experimental curves. In accordance with experiments, the intersubband absorption exhibits a longer lasting decay with respect to the bleaching. The calculated intersubband decay can be fitted with a monoexponential curve of 6 ± 1 ps, which is in the error interval of the average value from experiments (4.8 ± 1) ps, obtained from measurements on several 2-layer single flakes. The best fitting for the calculated bleaching decay is a biexpontial function with a first component of 0.2 ps

and a second of 2.3 ps also in this case in very good agreement with the experimental values reported in the inset of Fig. 3(a).

Figure 4 summarizes the carrier lifetimes extracted from the monoexponential decays of the intersubband transitions for single flakes differing in the number of stacked layers. Transient absorption decay for the 10- and 15-layer samples are recorded at 0.65 eV where the spectra exhibit intersubband transitions. The complete spectra are reported in [9]. Within our uncertainties we observe carrier lifetime values ranging from 4 to 6 ps for samples up to 4 layers. For thicker samples made of 5, 10, and 15 layers, which should be more representative for graphite, lifetime values are shorter and close to 3 ps. Because of the absence of subbands in 1-layer graphene, the method proposed here cannot be applied to this material system. Therefore, other experiments, for example, based on transient photoconductivity have to be optimized in order to extract values for 1-layer graphene [25]. Nevertheless, we want to emphasize that the approach used here is contactless and avoids the typical problems of time resolved photoconductivity such as carrier sweep out time or potential energy barriers potentially generated at metal-graphene contacts. In addition, we would like to point out the differences and advantages with respect to other powerful contactless methods to access carrier lifetime such as optical-pump terahertz-probe time resolved spectroscopy. Because of the low photon energy of terahertz pulses (1.6 to 6 meV) it is possible to measure the Drude intraband absorption of the carriers almost independently from their **k** value. However, the cross section or signal strengths related to this process may be not as high as for those of the intersubband transitions probed in our experiments. We also note that terahertz radiation has a wavelength which is typically above 200 μm and thus difficult to focus at dimensions comparable to those of mechanical exfoliated flakes (tens of μm range). Indeed, most of the experiments reported so far using terahertz radiation were performed on large area epitaxially grown flakes [20,26].
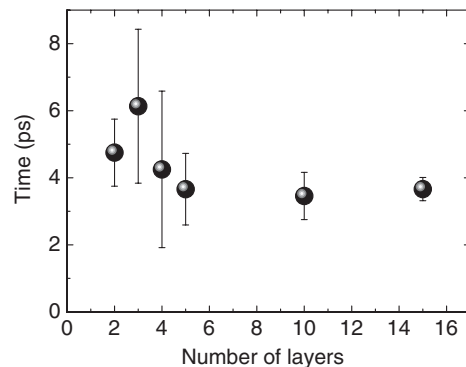
FIG. 4. Experimentally determined carrier lifetime as a function of the number of layers in several few layer graphene samples starting from 2 layer up to 15 layer. Error bars represent standard deviation obtained from several decay curves.

In conclusion, we have measured the carrier lifetime in a class of semimetals such as few-layer graphene. The gapless nature of these materials does not allow for using the typical optical methods to determine carrier lifetimes. We have demonstrated that intersubband transitions in the midinfrared part of the spectrum can be used to monitor the lifetime of hot carriers which ranges from 4 to 6 ps for few layer graphene and appears to be longer than those in epitaxial graphene [20] and graphite. These lifetimes should still allow us to build optoelectronic and photonic devices with modulation speeds up to 200 GHz.

*edc25@bath.ac.uk

[1] P. T. Landsberg, *Recombination in Semiconductors* (Cambridge University Press, Cambridge, England, 2003).

[2] S. Raghu, X. L. Qi, C. Honerkamp, and S. C. Zhang, Phys. Rev. Lett. **100**, 156401 (2008).

[3] A. H. Castro Neto, F. Guinea, N. M. R. Peres, K. S. Novoselov, and A. K. Geim, Rev. Mod. Phys. **81**, 109 (2009).

[4] T. Mueller, F. Xia, and P. Avouris, Nat. Photonics **4**, 297 (2010).

[5] F. Bonaccorso, Z. Sun, T. Hasan, and A. C. Ferrari, Nat. Photonics **4**, 611 (2010).

[6] M. Liu, X. Yin, E. Ulin-Avila, B. Geng, T. Zentgraf, L. Ju, F. Wang, and X. Zhang, Nature (London) **474**, 64 (2011).

[7] B. Partoens and F. M. Peeters, Phys. Rev. B **74**, 075404 (2006).

[8] K. F. Mak, M. Y. Sfeir, J. A. Misewich, and T. F. Heinz, Proc. Natl. Acad. Sci. U.S.A. **107**, 14 999 (2010).

[9] See Supplemental Material at http://link.aps.org/supplemental/10.1103/PhysRevLett.110.217406 for

[10] Y. Y. Wang, Z. h. Ni, T. Yu, Z. X. Shen, H. m. Wang, Y. h. Wu, W. Chen, and A. T. S. Wee, J. Phys. Chem. C **112**, 10 637 (2008).

[11] L. M. Malard, M. A. Pimenta, G. Dresselhaus, and M. S. Dresselhaus, Phys. Rep. **473**, 51 (2009).

[12] A. Das *et al.*, Nat. Nanotechnol. **3**, 210 (2008).

[13] N. Jung, N. Kim, S. Jockusch, N. J. Turro, P. Kim, and L. Brus, Nano Lett. **9**, 4133 (2009).

[14] R. Tautz *et al.*, Nat. Commun. **3**, 970 (2012).

[15] S. W. Koch and H. Haug, *Quantum Theory of the Optical and Electronic Properties of Semiconductors* (World Scientific, Singapore, 2004).

[16] T. Limmer, A. J. Houtepen, A. Niggebaum, R. Tautz, and E. Da Como, Appl. Phys. Lett. **99**, 103104 (2011).

[17] K. F. Mak, M. Y. Sfeir, Y. Wu, C. H. Lui, J. A. Misewich, and T. F. Heinz, Phys. Rev. Lett. **101**, 196405 (2008).

[18] S. Winnerl *et al.*, Phys. Rev. Lett. **107**, 237401 (2011).

[19] P. J. Hale, S. M. Hornett, J. Moger, D. W. Horsell, and E. Hendry., Phys. Rev. B **83**, 121404 (2011).

[20] P. A. George, J. Strait, J. Dawlaty, S. Shivaraman, M. Chandrashekhar, F. Rana, and M. G. Spencer, Nano Lett. **8**, 4248 (2008).

[21] F. Rana, J. H. Strait, H. Wang, and C. Manolatou, Phys. Rev. B **84**, 045437 (2011).

[22] F. Rana, Phys. Rev. B **76**, 155431 (2007).

[23] F. Rana, P. A. George, J. H. Strait, J. Dawlaty, S. Shivaraman, M. Chandrashekhar, and M. G. Spencer, Phys. Rev. B **79**, 115447 (2009).

[24] F. Rana, J. H. Strait, H. Wang, and C. Manolatou, Phys. Rev. B **84**, 045437 (2011).

[25] A. Urich, K. Unterrainer, and T. Mueller, Nano Lett. **11**, 2804 (2011).

[26] J. H. Strait, H. Wang, S. Shivaraman, V. Shields, M. G. Spencer, and F. Rana, Nano Lett. **11**, 4902 (2011).